JOURNAL OF THERMOPHYSICS AND HEAT TRANSFER
Vol. 17, No. 3, July–September 2003

Capillary Evaporation in Microchanneled Polymer Films

Y. X. Wang* and G. P. Peterson†
Rensselaer Polytechnic Institute, Troy, New York 12180

The capillary-driven evaporation heat transfer and the resulting fluid flow mechanisms occurring in a microchanneled, flexible polymer microfilm were investigated to better understand the operation and improve the design process of two-phase flexible membrane heat pipe devices. Experimental tests were conducted to evaluate the capillary evaporation heat transfer limit in a polymer microfilm with 26-μm-wide capillary grooves. The experimental results indicated that the microchanneled polymer film could create a capillary force sufficient to function adequately when used with wettable working fluids such as methanol or ethanol. The maximum evaporation heat transport capacity was found to decrease significantly as the effective length of the polymer microfilm increased. In addition to the experimental portion of the investigation, an analytical model was developed to predict the capillary evaporation limitation. When this model was used, the effects of variations in the geometric parameters of the microgrooves on the evaporation heat transfer were analyzed. The results indicated that when the half-angle of the trapezoidal grooves was fixed, the maximum evaporation heat transfer rate increased with increases in the depth and decreases in the width of the grooves. Predictions obtained from the analytical model were then compared with the results of the experimental investigation and indicated good agreement.

Nomenclature

$A_{c,l}$	=	liquid phase cross-sectional area, m^2
a	=	half-width of the bottom of the microgrove, m
D_h	=	hydraulic diameter of liquid, m
f	=	liquid friction factor
g	=	gravity acceleration, m/s^2
h_b	=	thickness of the base, m
h_{fg}	=	latent heat of vaporization, J/kg
h_g	=	height of the microgroove, m
h_v	=	height of the vapor channel, m
K	=	permeability, m^2
L	=	effective length of test article, m
L_a	=	length of the adiabatic section of the microfilm, m
L_e	=	length of evaporator section, m
L_{eff}	=	effective length of the microfilm, m
P_{cap}	=	capillary pressure, Pa
P_l	=	liquid pressure, Pa
p_l	=	wetted perimeter of channel, m
$Q_{\max}$	=	maximum heat transport capacity, W
q''	=	heat flux, W/m^2
$Re_{l,h}$	=	Reynolds number
r_m	=	radius of liquid meniscus, m
u_D	=	Darcy velocity, m/s
w	=	top width of the vapor channel, m
w_t	=	half top width of the microgroove, m
w_u	=	width of channel, m
w'	=	width between two vapor channels, m
α	=	contact angle, grade
θ	=	inclination angle, deg
μ_l	=	liquid viscosity, N · s/m^2
ν_l	=	liquid dynamic viscosity, m^2/s
ρ_l	=	liquid density, kg/m^3
σ	=	surface tension, N/m
ϕ	=	half-angle of the microgroove, grade

Subscripts

a	=	adiabatic
cap	=	capillary
e	=	evaporator
l	=	liquid phase
m	=	meniscus

Received 3 September 2002; accepted for publication 1 April 2003.

*Research Assistant Professor, Department of Mechanical, Aeronautical and Nuclear Engineering. Member AIAA.

†Professor of Aerospace, Mechanical and Nuclear Engineering, Department of Mechanical, Aeronautical and Nuclear Engineering. Fellow AIAA.

Introduction

HEAT pipes fabricated from thin, flexible microfilms have considerable potential for use in applications in the aerospace, microelectronic, and medical industries. These applications, however, require a fundamental understanding of the heat transfer and fluid flow mechanisms occurring in the wick structures of these devices. As presented in a previous investigation,[1] a thin, flexible polymer membrane heat pipe has been designed, modeled, and fabricated using a microchanneled polymer films manufactured by the 3M Corporation.[2] Because the evaporation and condensation heat transfer occurring in the microgrooves play a vital role in the operation of the heat pipe, it is necessary to understand the mechanisms that govern the evaporation and condensation in these devices and the various limitations that occur.

The capillary evaporation heat transport capacity in microgrooves is governed by the capillary limit, which occurs when the total pressure drop along the liquid flow path exceeds the capillary pumping ability of the wick structure, or in this case the microgrooves, preventing the liquid from being continuously supplied to the evaporator. Most of the previous research in this area has focused on single- or two-phase flow in larger, more conventional-sized channels with or without enhanced inner or outer surfaces.[3] However, as the power requirements, size, and flexibility constraints in microelectronic systems, spacecraft, and medical apparatus all increase, the development of these devices will become increasingly important.

Classical theory indicates that as the size of the channels and the feature size of an enhanced surface decrease, the surface exhibits a greater tendency to remain wet, even at higher applied heat fluxes. This is the result of the molecular forces that exist in very thin liquid layers. At critically high heat fluxes, the fluid vaporizes very quickly, resulting in a very thin liquid film on the surface of the evaporator. As this film thins, the forces become increasingly stronger. Because the thickness of the film is often related to the channel or feature size, enhanced surfaces with miniature- to micro-sized dimensions will remain wetted at higher heat fluxes than larger, conventionally sized surfaces, due to the increased effects of capillary, surface tension, and disjoining forces.

Investigations into the effects of miniaturization have been undertaken recently to facilitate applications in high heat flux cooling devices, but considerable work remains to be done. Bowers and Mudawar[4] experimentally investigated the critical heat flux and pressure drop in smooth mini- and micro-copper channels with diameters of 2.54 and 0.51 mm, respectively. The working fluid in this investigation was R113. The results demonstrated critical heat flux values in excess of 200 W/cm^2, when applied to a single surface of the heat sink, at modest flow rates and pressure drops. The results further demonstrated that the inlet subcooling effects were negligible and that minichannels were favorable to microchannels in that comparable heat fluxes were achieved with much lower pressure drops and reduced manufacturing complexity. However, for both ranges of channel size, a uniform wall superheat of 100°C occurred at higher heat fluxes, resulting in a large thermal resistance for the smooth walled heat sinks. Bowers and Mudawar[4] also presented a homogenous two-phase pressure drop model based on the total mass flow rates. The model accounted for the total pressure gradient as the sum of the contributions from friction and acceleration. The model was accurate to within 30% of all experimental data presented. In this investigation, it was determined that the acceleration contributed 75–90% of the total pressure drop over the boiling region.

Yang and Webb[5] conducted experimental tests and modeled the pressure drop across plain rectangular and enhanced shallow microfinned tubes (0.4 mm wide and 0.2 mm deep) with hydraulic diameters of 2.64 and 1.56 mm, respectively. The predicted frictional pressure drop was shown to be in good agreement with the experimental data, with all values falling within 20%. It was further shown that the pressure drop in both tubes was dominated by the vapor shear. This result was confirmed by Peng and Peterson,[6] who experimentally investigated the single-phase convection heat transfer and fluid flow in microchannel structures with widths of 0.1–0.4 mm.

In addition to these experimental investigations, fundamental analytical investigations of the evaporation heat transfer processes in microchannels have also been conducted in recent years. These investigations include the thin film evaporation processes,[7–9] the capillary fluid flow and heat transfer,[10–12] and the evaporating stability in the microchannels/grooves.[13]

As seen from the preceding summary, the vast majority of the research conducted to date, has focused on forced convection heat transfer, fluid flow, and phase-change phenomena in channel widths larger than 0.1 mm. Little or no research has been done on the evaporation process in capillary-induced flow in flexible polymer microchannels of the range of 20–30 μm. As a result, the current study will play a fundamental role in the development and optimization of flexible film heat pipes/spreaders or radiators for microelectronic systems, spacecraft, and medical applications.

The objectives of this investigation focus on the experimental investigation and modeling of the capillary evaporation limitation of microgrooved polymer films with different working fluids. In addition, the effects of the geometric configuration on the capillary evaporation heat transfer limitation and required superheat are also investigated to support and develop an optimum design of the microstructures.

Experimental Facility and Procedures

An experimental test facility was developed to measure the capillary evaporation performance of the micro-polymer film with different potential working fluids. The experimental test facility is shown in Fig. 1. The experimental system included a vacuum chamber and system, a thermal heating/cooling system, the test article, a liquid supply system, and a data acquisition system. The test article was prepared by attaching a small section of the microfilm (25.4 × 152.4 mm), shown in Fig. 2, to a flat aluminum plate, as shown in Fig. 3. A thin film electric heater, which measures by 25.4 × 25.4 mm, was attached to the ungrooved side of the polymer film. The bottom side of the heated area was insulated to reduce the heat loss through conduction and convection. Four thermocouples were attached to the bottom surface of the film heater, and six

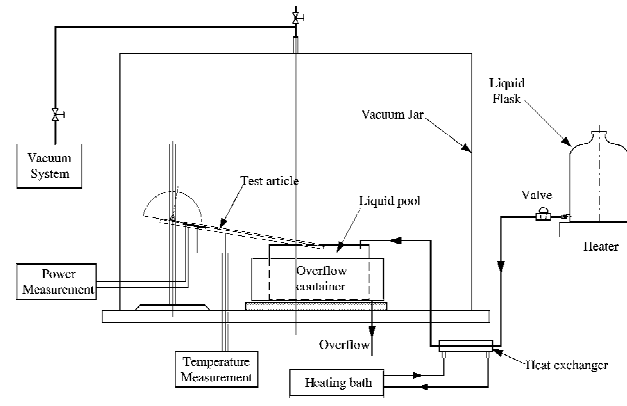

Fig. 1 Schematic of the experimental test facility.

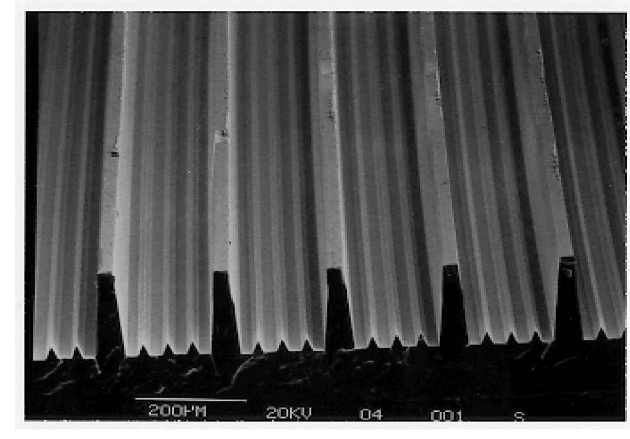

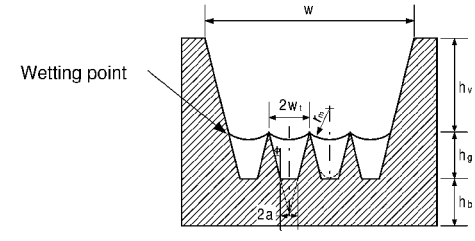

Fig. 2 Microchanneled film.[2]

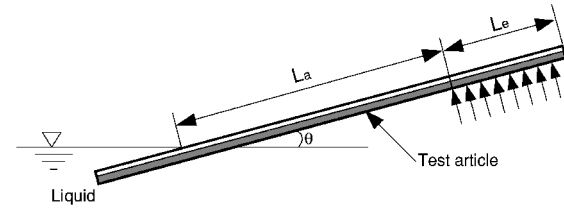

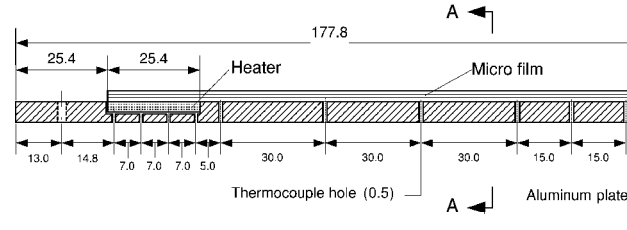

Fig. 3 Schematic of the test article instrumentation.

thermocouples were installed on the back surface of the adiabatic section of the polymer film through small holes in the aluminum plate. These six thermocouples were used to monitor the temperature along the test article and were located as illustrated in Fig. 3. The thermocouples were T type (AWG-36) with an uncertainty of $\pm 0.5^{\circ}$C as provided by the manufacturer. Because the thermocouples in the evaporator section were attached to the backside of the film heater, it was necessary to consider the thermal resistance of the heater in computing the temperature at the polymer surface.

The test article was supported in such a manner that the tilt angle could be adjusted. One end of the test article was lowered into the container with the working fluid and the thin film heater was attached to the other end. The overall length of the adiabatic section was controlled by varying the length of the test article that was immersed in the fluid.

The liquid flow system used for the working fluid was designed and fabricated as an overflow type, in which the extra liquid overflows into the collecting pool. The working fluid from the liquid flask flowed through a double pipe heat exchanger and into the overflow container, where it was heated to the required temperature by a constant temperature thermal bath. The liquid level and temperature were both held constant through out all of the tests.

All tests were conducted in a vacuum chamber in which the vapor-phase temperature was maintained at the saturation temperature using a temperature controller and electric heater bonded to the bottom and sides of the chamber. Power was supplied to the heater by an autotransformer and measured with a pair of multimeters connected to an automated data acquisition system. All temperatures were monitored, measured, and recorded using an automated data acquisition system.

All of the experiments were carried out using the following procedure. The test device was placed on the bottom of the vacuum chamber, the tilt angle was adjusted, and the adiabatic length of the test article was set to the required configuration. Before the test, the vacuum chamber was evacuated to remove the air, and then the valve to the vacuum pump was closed. The working fluid from the high-level flask flowed through the two-tube heat exchanger and was heated to the required saturation temperature by circulating through the constant temperature bath. The working fluid was allowed to flow into the overflow container, and the pressure in the vacuum chamber was set to the saturation pressure corresponding to the working fluid temperature. The working fluid that overflowed was collected in the outer flask and returned to the liquid flask. When the environment in the vacuum chamber reached equilibrium conditions, the autotransformer was turned on, and the power to the heater was adjusted, and the temperatures on the test article and the temperature of the liquid pool were recorded. The power input was incremented until the temperature at the end of the evaporator increased sharply and dryout occurred. When the system reached equilibrium, that is, the temperature variations occurring in the test article were less than 0.1°C in 30 min, the length of the adiabatic section was adjusted by lowering the test article into the liquid reservoir to determine the maximum evaporation heat transfer for different lengths. Tests were conducted at 5-, 10-, and 20-deg angles with respect to the horizontal.

Analysis

As the fluid in the evaporator is vaporized, the liquid interface recedes into the grooves, forming a curvature due to the surface tension, as shown in Fig. 2. The working fluid in the liquid pool is pumped back into the channel by the capillary pressure created by this liquid curvature. As described by the Young–Laplace equation, the smaller the meniscus radius is, the higher the capillary pressure. This would imply that smaller channels are better; however, the decrease in the size of the microchannel results in an increase in the flow resistance. To maintain the continuity of the interfacial evaporation, the frictional pressure drop resulting from the liquid flow in the microstructure must be less than the capillary pressure produced by the capillary structure. When the liquid frictional pressure drop is equal to the capillary pumping pressure, the evaporation heat transfer reaches maximum value, that is,

$$\Delta P_l = \Delta P_{\text{cap}} \tag{1}$$

The capillary pressure can be estimated by the Young–Laplace equation and expressed as

$$\Delta P_{\text{cap}} = \sigma \cos\alpha / r_m \tag{2}$$

For the film shown in Fig. 2, it is appropriate to treat the fluid flow as a one-dimensional problem. Because the velocity and Reynolds number of liquid flow in the microchannels is very small, the convective terms in the momentum equation can be neglected, and the liquid pressure gradient along the microchannel can be calculated by Darcy's law as

$$-\frac{\mathrm{d}P_l}{\mathrm{d}z} = \frac{\mu_l u_D}{K} + \rho_l g \sin\theta \tag{3}$$

where K is the permeability of the trapezoidal microfilm and can be expressed as

$$K = \frac{D_h^2 \varepsilon}{2(f_l Re_{l,h})} \tag{4}$$

The friction factor, $f_l Re_{l,h}$, in Eq. (4) can be obtained from the literature[14] for the trapezoidal configuration. The porosity of the microfilm, ε, is dependant on the geometry of the grooves and the liquid distribution profile in the microchannels. The Darcy velocity in Eq. (3) can be obtained from the energy conservation equation as

$$A_{c,l}\rho_l \frac{\mathrm{d}u_D}{\mathrm{d}z} - \frac{q'' w'}{h_{fg}} = 0 \tag{5}$$

and rearranging Eq. (5) yields

$$\frac{\mathrm{d}u_D}{\mathrm{d}z} = \frac{q'' w'}{A_{c,l}\rho_l h_{fg}} \tag{6}$$

where $A_{c,l}$ is the cross-sectional area of the microchannel and is a function of the meniscus radius of the liquid surface.

Assume the velocity of the liquid phase at the end of the evaporator section ($z = 0$) is zero, then the velocity on the evaporation section is

$$u_D = \frac{q'' w' z}{A_{c,l}\rho_l h_{fg}} \tag{7}$$

and the Darcy velocity in the adiabatic section is held constant as

$$u_D = \frac{q'' w' L_e}{A_{c,l}\rho_l h_{fg}} \tag{8}$$

Substituting Eqs. (7) and (8) into Eq. (3) and integrating to find the wet point in the evaporator end yields

$$\Delta P_l = \frac{q'' w' \mu_l L_e}{A_{c,l} K \rho_l h_{fg}} L_{\text{eff}} + \rho_l g L \sin\theta \tag{9}$$

When Eqs. (2) and (9) are combined, the liquid flow criterion required to maintain continuous interfacial evaporation yields

$$q''_{\max} = \left(\frac{\sigma \cos\alpha}{r_m} - \rho_l g L \sin\beta \right) \frac{A_{c,l} K h_{fg}}{w' \gamma_l L_e L_{\text{eff}}} \tag{10}$$

where L_{eff} is the effective length of the film, defined as

$$L_{\text{eff}} = 0.5 L_a + L_e \tag{11}$$

and L is the length from the wet point to the end of the evaporator section,

$$L = L_a + L_e \tag{12}$$

Results and Discussion

Experimental tests were conducted on a series of test articles fabricated from a polymer film manufactured by 3M Corporation.[2] The geometric configuration of this microfilm is presented in Table 1. When the power input to the evaporator section and the temperatures along the axial length of the test article were measured, the maximum evaporation heat transfer was obtained for different lengths and various tilt angles. Because of the high wettability of the working fluid for this particular polymer film, methanol and ethanol were chosen as the working fluids. As expected, the maximum evaporation heat transfer rate of the microfilm described was strongly affected by the length of the film, operating temperature, and tilt angle. The experimental results of the maximum evaporation heat transfer are shown in Fig. 4 for methanol and ethanol at a tilt angle of 10 deg. It is clear that the maximum evaporation heat transfer of the microfilm decreases rapidly with increases in the length of the test article. (The length of the evaporator was held constant.) In addition, higher evaporation heat transfer rates were obtained for methanol than for ethanol.

Increasing the tilt angle resulted in a negative effect on the maximum evaporation heat transfer due to the effect of gravity. The experimental results obtained for methanol are shown in Fig. 5. The length of the test section was 76.2 mm. As illustrated, the maximum evaporation heat transfer decreased slowly with increasing tilt angle.

When the model developed earlier is used, the maximum capillary evaporation heat transfer can be predicted. However, the liquid cross-sectional area and the wetted perimeter of the channel depend on the profile of the liquid meniscus and the position along the film. The evaporation rate is very sensitive to these parameters. Two different models, each using different liquid fill charges and assumptions, were developed and compared with the experimental results to determine which one could most accurately predict the operational limits and performance characteristics.

When it is assumed that the working fluid only fills the microgrooves and the minimum meniscus radius of the liquid surface is reached when the liquid surface approaches the bottom surface

Table 1 Physical dimensions of the microfilm[2]

Parameter	Value
W', μm	300
W, μm	268
W_t, μm	23.5
A, μm	13
h_v, μm	134
h_g, μm	26
h_b, μm	100
ϕ, deg	22
k, W/m · K	0.33

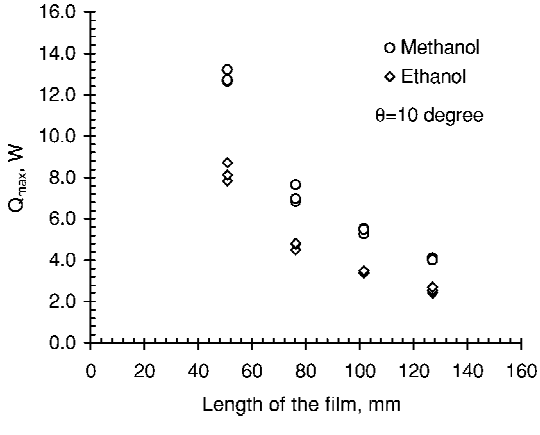

Fig. 4 Maximum evaporation heat transfer with length variation at θ = 10 deg.

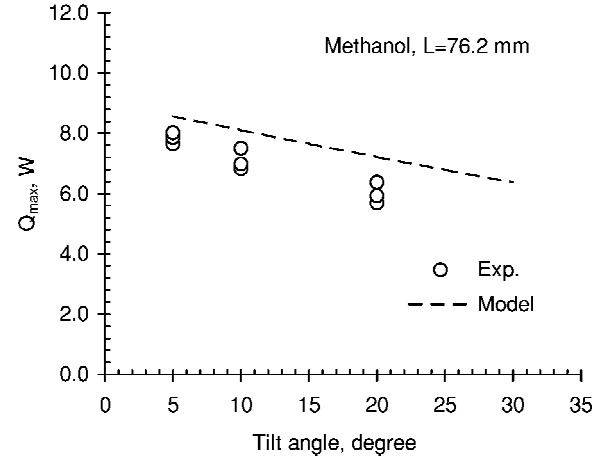

Fig. 5 Influence of tilt angle on maximum evaporation heat transfer of the microgrooved film with L = 76.2 mm.

of the micro grooves, the minimum radius can be estimated as[15]

$$r_{m,\min} = \frac{w_t - h_g \tan\phi}{\cos(\phi + \alpha_0) - \tan\phi[1 - \sin(\phi + \alpha)]} \tag{13}$$

and the liquid cross-sectional area and wetted perimeter can be obtained as

$$A_{c,l} = 2(3w_t + a + h_g \tan\phi')h_g \tag{14}$$

$$p_l = 2h_g\left(\frac{3}{\cos\phi} + \frac{1}{\cos\phi'}\right) + 8a \tag{15}$$

$$\varepsilon = \frac{3w_t + 5a + h_g \tan\phi'}{2(3w_t + a + h_g \tan\phi')} \tag{16}$$

This is model 1.

When it is assumed that the working liquid completely fills the microgrooves and protrudes into the vapor channel, that is, flooding the space area above the microgrooves, in the adiabatic section and recedes into the microgrooves at the end of the evaporator section, the minimum liquid meniscus radius is reached when the meniscus recedes into the micro grooves. While creating higher capillary pressure, the liquid artery area decreases significantly in the evaporation section. The liquid profile is affected by the structure and the pressure difference. The cross-sectional area of the liquid varies from the evaporator section to the wetting point. In model 2 the liquid cross-sectional area is calculated from the radius of the curvature. For the smaller channel, the liquid profile has a significant effect on the cross-sectional area of the liquid phase and, therefore, affects the heat transfer performance. The liquid cross-sectional area and the wetted perimeter in the vapor channel can be expressed as

$$A_{c,l} = \frac{\left\lfloor (r_m \sin\varphi')^2 - (3w_t + a)^2 \right\rfloor}{\tan\phi'} - r_m^2(\varphi' - \sin\varphi'\cos\varphi') - 3(w_t - a)h_g \tag{17}$$

$$p_l = \frac{2(r_m \sin\varphi' - a)}{\sin\phi'} + 8a + \frac{6h_g}{\cos\phi'} \tag{18}$$

where $\varphi' = (\pi/2) - \phi' - \alpha$.

The modeling results are presented in Figs. 6a and 6b for methanol with tilt angles of 5 and 10 deg, respectively. In addition, the experimental results are presented and compared. As illustrated, the maximum evaporation heat transfer rate predicted by model 1 is much lower than the values predicted by model 2. Comparison of the experimental results with the modeling results clearly indicates that model 2 is superior and can be used to accurately predict the capillary evaporation limitation of the microfilm. The validity of the

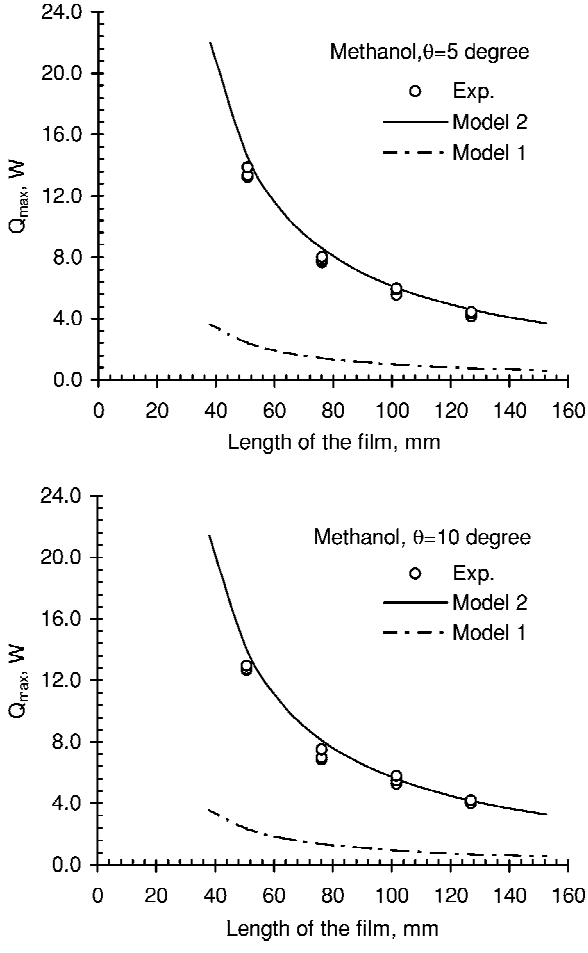

Fig. 6 Comparison of modeling and experimental results of maximum evaporation heat transfer of microgrooved film.

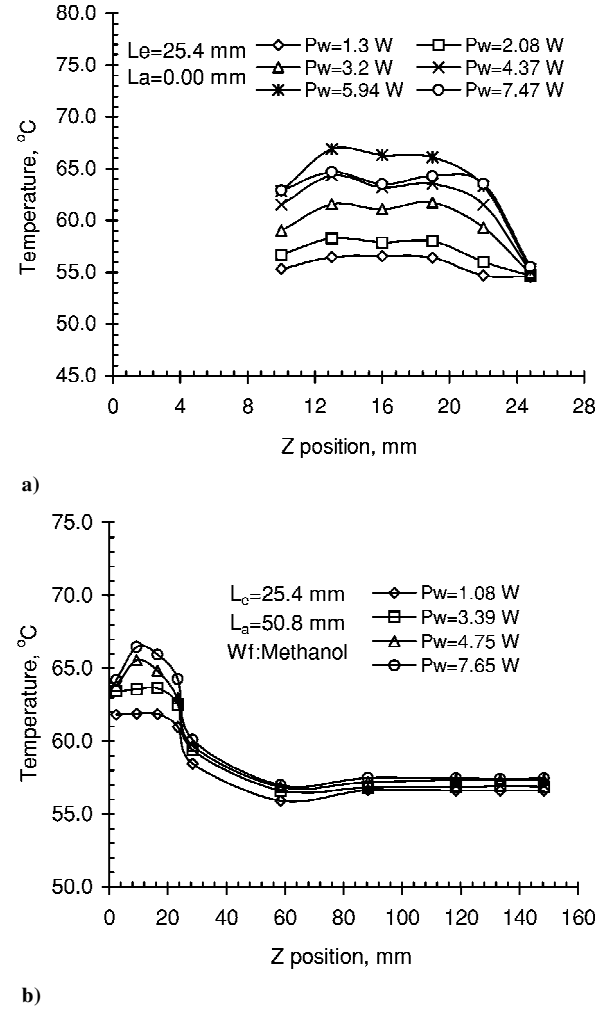

Fig. 7 Temperature distributions on microgrooved film with methanol as working fluid.

model is also verified in Fig. 6 for methanol with the variation of the tilt angle.

The assumption of the liquid meniscus variation along the microchannels in model 2 can also be verified by the observed temperature variation on the evaporation section. As an example, two observed temperature distributions on the test article are shown in Fig. 7. The data in Fig 7a. are from experimental tests conducted by Zhang.[16] When the heat flux added in the evaporation section approached the dryout point, the temperature at the far end of the evaporator dropped dramatically, and the highest temperature occurred at the next point along the axial length. This indicates that, as the liquid interface recedes into the microgrooves at the end of the evaporator and the liquid meniscus becomes very thin, the thermal resistance through the liquid film becomes smaller. As a result, the required temperature difference is smaller for uniform heat flux conditions.

Based on the preceding analysis, model 2 can be employed to predict accurately the evaporation performance of the microfilm. Some modeling results of capillary evaporation performance of the microfilm and the effects of the geometric parameters, as well as properties of the working fluid, follow. Because physical properties and the wettability of the working fluid can vary, the capillary evaporation performance of the microfilm is different. Figure 8 shows the modeling results of the maximum capillary evaporation heat transfer for methanol and ethanol. Apparently, the thermophysical properties of the methanol make it superior in terms of performance to ethanol.

For the trapezoidal configuration studied here, the top and bottom widths of the groove have a significant effect on the capillary evaporation performance through the determination of the minimum liquid meniscus radius and the liquid cross-sectional area. As shown in Fig. 9, as the bottom width of the microgroove becomes smaller,

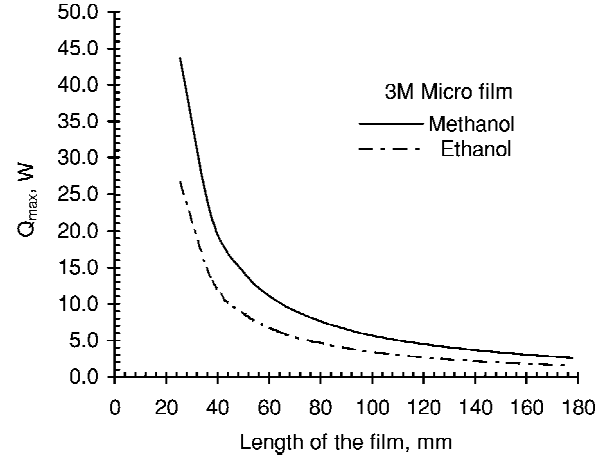

Fig. 8 Modeling results of maximum evaporation heat transfer of microgrooved film with methanol and ethanol as working fluids.

the capillary evaporation heat transfer increases significantly. However, the increase in the top width of the trapezoidal groove results in a decrease in the heat transfer performance. This means that the sharp corner ($a = 0$) or a triangular shape with a large aspect ratio is favorable to capillary evaporation. The effect of the half-angle of the microgroove on the evaporation performance is shown in Fig. 10. For different sizes of grooves, the effect is different, but for every case, there exists an optimum tilt angle for the microfilm at which

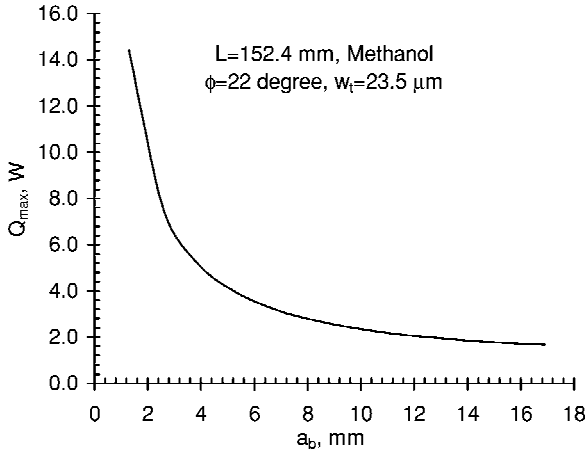

Fig. 9 Effect of the bottom width of the microgroove on maximum evaporation heat transfer of microgrooved film.

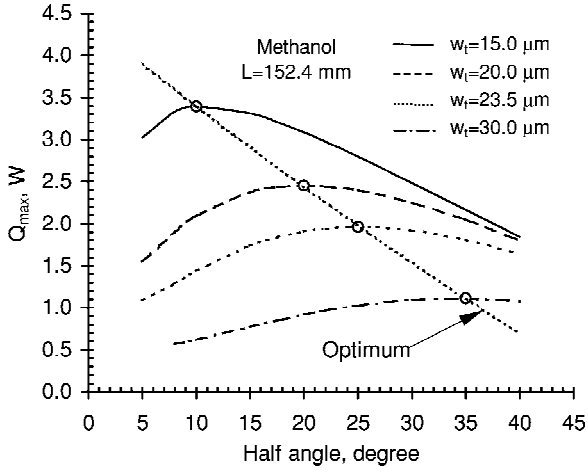

Fig. 10 Effect of half-angle of microgroove on maximum evaporation heat transfer of microgrooved film.

the groove size and shape are optimal and the capillary performance is maximized.

Note that the evaporation heat transfer in the microchannel film is different from the heat transfer phenomena occurring in the heat pipe device constructed from this material. The liquid distribution and profile depends on the charge of the working fluid in the heat pipe, and because of the free liquid surface, the working fluid will assume a shape governed by this free surface energy. The shape of the liquid can be determined by minimizing the free surface energy of the liquid–vapor interface.

Conclusions

Experiments were conducted to measure the capillary evaporation limitations of a polymer film with microchannels. The experimental results indicated that the maximum evaporation heat transfer was significantly affected by the effective length of the microfilm and decreased rapidly with increasing film length. The tilt angle, as expected, had a negative effect on the evaporation performance. Experimental observations of the temperature variations indicated that minimum liquid meniscus radius occurs in the microgrooves just before dryout. Tests were conducted using both methanol and ethanol, and both were found to be good candidates for use as potential working fluids for this application.

Two analytical models were developed to evaluate the capillary evaporation heat transfer on the microfilm. The effect of geometric parameters on the evaporation heat transfer performance of the microfilm was studied, and the results indicated that, for the trapezoidal grooves, decreasing the bottom width of the groove very slightly can significantly improve the evaporation heat transfer performance. When the analytical models are used, the optimal half-angle of the groove can be determined to optimize the heat transfer performance.

Comparison of the models with the experimental results clarified the fluid behavior in the adiabatic section of the film and indicated very good agreement between model 2 and the experimentally obtained results for a given set of conditions.

Acknowledgments

The authors acknowledge the support of the National Science Foundation, Lockheed Martin Missiles and Fire Control Corporation, and the Office of Naval Research for their support of this work and 3M Corporation for supplying the film materials.

References

[1]McDaniels, D., and Peterson, G. P., "Investigation of Polymer Based Micro Heat Pipes For a Flexible Spacecraft Radiator," *Proceedings of 2001 ASME International Mechanical Engineering Conference and Exposition*, Vol. 124, American Society of Mechanical Engineers, New York, 2001.

[2]Johnston, R. P., Fehr, R. T., and Servatius, J. A., "Liquid Management Films for Absorbent Articles," U.S. Patent 5,728,446, 23 Oct. 1995.

[3]Plam, B., "Heat Transfer in Microchannels," *Microscale Thermophysical Engineering*, Vol. 5, No. 3, 2001, pp. 155–175.

[4]Bowers, R., and Mudawar, I., "High Heat Flux Boiling in Low Flow Rate, Low Pressure Drop Mini-Channel and Micro-Channel Heat Sinks," *International Journal of Heat and Mass Transfer*, Vol. 37, No. 2, 1994, pp. 321–332.

[5]Yang, C. Y., and Webb, R. L., "Friction Pressure Drop of R-12 in a Small Hydraulic Diameter Extruded Tubes with or without Micro-fins," *International Journal of Heat and Mass Transfer*, Vol. 39, No. 4, 1996, pp. 801–809.

[6]Peng, X. F., and Peterson, G. P., "Convective Heat Transfer and Flow Friction for Water Flow in Microchannel Structures," *International Journal of Heat and Mass Transfer*, Vol. 39, No. 12, 1996, pp. 2599–2608.

[7]Wayner, P. C., Kao, Y. K., and LaCroix, L. V., "The Interline Heat Transfer Coefficient of an Evaporating Wetting Film," *International Journal of Heat and Mass Transfer*, Vol. 19, No. 1, 1976, pp. 487–492.

[8]Ha, J. M., and Peterson, G. P., "The Interline Heat Transfer of Evaporating Thin Films Along a Micro Grooved Surface," *Journal of Heat Transfer*, Vol. 118, No. 3, 1996, pp. 747–755.

[9]Ma, H. B., and Peterson, G. P., "Temperature Variation and Heat Transfer in Triangular Grooves with Evaporating Film," *Journal of Thermophysics and Heat Transfer*, Vol. 11, No. 1, 1997, pp. 90–97.

[10]Khrustalev, D. R., and Faghri, A., "Heat Transfer During Evaporation on Capillary Grooved Structures of Heat Pipes," *Journal of Heat Transfer*, Vol. 117, No. 3, 1995, pp. 740–747.

[11]Ma, H. B., and Peterson, G. P., "Experimental Investigation of Maximum Heat Transfer in Triangular Grooves," *Journal of Heat Transfer*, Vol. 118, No. 3, 1996, pp. 740–746.

[12]Peterson, G. P., and Ha, J. M., "Capillary Performance of Evaporating Flow in Micro Grooves: An Approximate Analytical Approach and Experimental Investigation," *Journal of Heat Transfer*, Vol. 120, No. 3, 1998, pp. 743–751.

[13]Kennedy, J. E., Roach, G. M., Dowling, M. F., Abdel-Khalik, S. I., Ghiaasiaan, S. M., Jeter, S. M., and Quershi, Z. H., "The Onset of Flow Instability in Uniformly Heated Horizontal Microchannels," *Journal of Heat Transfer*, Vol. 122, No. 1, 2002, pp. 118–125.

[14]Shah, R. K., and Bhatti, M. S., "Laminar Convective Heat Transfer in Ducts," *Handbook of Single-Phase Convective Heat Transfer*, Wiley, New York, 1987, pp. 3.70–3.71.

[15]Hopkins, R., Faghri, A., and Khrustalev, D., "Flat Miniature Heat Pipes with Micro Capillary Grooves," *Journal of Heat Transfer*, Vol. 121, No. 1, 1999, pp. 102–109.

[16]Zhang, J. T., "Experimental Investigation on Thin Film Evaporation," ONR Progress Report 01-000140010454, submitted to the Office of Naval Research, Arlington, VA, July 2001.